Article

Achieving High Dispersion of Pd in Small-Pore Zeolite SSZ-13: A High-Efficiency Low-Temperature NOx Adsorber

Yatao Liu,* Kaixiang Li, Yuankai Shao, Xiaoning Ren, Bingjie Zhou, Anqi Dong, Xi Liu, Cheng Lv, and Zhenguo Li*

Cite This: *ACS Omega* 2024, 9, 30452–30460

Read Online

ACCESS | Metrics & More | Article Recommendations | Supporting Information

ABSTRACT: Passive NO_x adsorber (PNA) materials are primarily considered for reducing nitrogen oxide emissions during the low-temperature cold start of a motor vehicle. Pd/SSZ-13 has attracted considerable attention because of its outstanding hydrothermal stability and sulfur resistance. Optimizing the dispersion of precious metal Pd in Pd/SSZ-13 is crucial for enhancing PNA performance and nitrogen oxide adsorption capability. In this study, we prepared Pd/SSZ-13 using different methods and evaluated their influence on the NO_x adsorption capability. The characterization results show that the dispersion of precious metal Pd in the Pd/SSZ-13 catalyst prepared by the quantitative ion-exchange method is as high as 92.13%, and the loading amount is as high as 98.93%. Pd predominantly exists as Pd^{2+}, achieving near-total loading and further improving the catalyst's NO_x adsorption capacity. This study offers innovative approaches and methods for applying Pd/SSZ-13 as a PNA material, serving as a reference for its further optimization and performance enhancement. Continued research into the preparation and adsorption performance of Pd/SSZ-13 materials could offer solutions to reduce motor vehicle nitrogen oxide emissions.
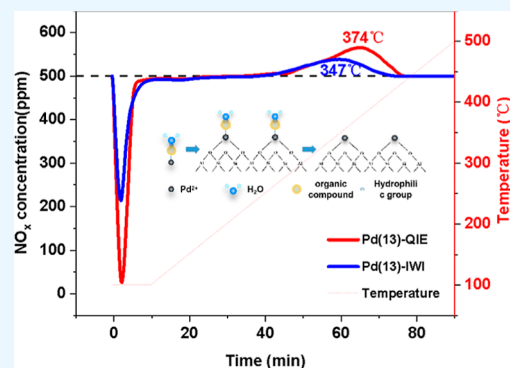
1. INTRODUCTION

Due to recent rapid economic development, China has seen a continuous increase in motor vehicles. Consequently, the environmental pollution caused by fuel combustion has received increasing attention. Vehicle exhaust emissions cause serious damage to the atmospheric environment, of which NO_x is the most prominent.[1−5] Therefore, De-NO_x (denitration) has become an important research topic worldwide. The contribution rate of NO_x emitted during the cold start of diesel vehicles exceeds 80%, which makes the control of NO_x emissions from diesel vehicle exhaust difficult.[6] With the strengthening of China VI emission regulations and the approach of China VII ultralow emission regulations, promoting the reduction of NO_x emissions during the cold-start phase is urgently required.[7−9]

The treatment of NO_x at low exhaust temperatures is challenging due to the limited effectiveness and poor denitrification efficiency of selective catalytic reduction (SCR) catalysts under these conditions.[10−12] Passive NO_x adsorption, efficiently adsorbing and desorbing NO_x at low and high temperatures, respectively, is increasingly viewed as a promising approach to tackle NO_x emissions during low-temperature cold start-ups. Currently, PNA materials are considered to be the most promising technology for addressing NO_x emissions during low-temperature cold start-ups.[6,13−15] Pd-modified zeolite PNA materials are attracting increasing attention because of their excellent NO_x storage capacity, resistance to poisoning, and hydrothermal stability and have become some of the most

promising PNA candidates.[14,16,17] Despite many advantages of Pd/zeolite PNA materials, their NO_x adsorption capacity still cannot meet practical needs; therefore, further improvement of catalyst adsorption performance is required. Zheng[18] and Konstantin et al.[19] demonstrated that atomically dispersed Pd primarily acts as the active adsorption site at the cation sites of zeolites, while PdO_2 and PdO particles are distributed on the zeolite's outer surface. This improved the dispersion of Pd and reduced the amount of PdO_2 and PdO particles on the zeolite surface. Consequently, the improved utilization rate of Pd can further enhance the NO_x storage capacity of Pd/zeolite. Highly dispersed Pd on zeolite-exchange sites serves as an active site for low-temperature NO storage.[20,21] A key challenge in developing high-performance PNAs is enhancing the number and dispersion of effective adsorption sites. If the zeolite's pore size is smaller than or similar to the size of the loaded metal species, diffusion into the pores is hindered. Introducing metal ions into small-pore zeolites using traditional methods is thus challenging.[22,23] Many researchers agree that heat treatment is an effective way to prepare Pd/SSZ-13 catalysts with highly
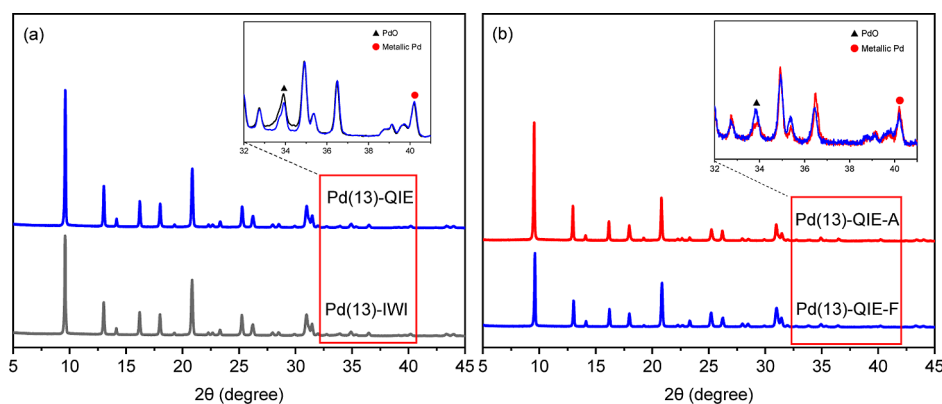
Figure 1. XRD patterns of (a) Pd(13)-IWI and Pd(13)-QIE and (b) Pd(13)-QIE before and after aging.

dispersed Pd ions. Hydrothermal aging can increase the migration rate of PdO within the zeolite, leading to the redistribution and formation of Pd^{2+} ionic species in SSZ-13, which enhances the NO adsorption capacity. However, this approach can degrade the zeolite framework to a certain extent.[24,25] It has been widely acknowledged that improving Pd dispersion in Pd/zeolites boosts their NO_x storage capacity, making the study of methods to enhance Pd dispersion in zeolites crucial.[26,27]

In this study, Pd/SSZ-13 samples with similar theoretical loadings were prepared using incipient wetness impregnation and quantitative ion-exchange methods. This was done to examine how different preparation techniques impact the low-temperature cold-start NO_x passive adsorption performance of Pd-loaded small-pore zeolites. We thoroughly investigated the NO_x adsorption/desorption behavior and PNA performance of Pd/SSZ-13 catalysts prepared via these methods, including their aging resistance assessed with a rapid aging device. The NO_x adsorption and desorption capabilities of both PNA material types were tested under simulated diesel engine exhaust conditions. Furthermore, we conducted a comprehensive analysis of the effects of the preparation methods on the physical and chemical states of Pd using characterization techniques such as scanning transmission electron microscopy (STEM), X-ray diffraction (XRD), BET surface area (BET), X-ray photoelectron spectroscopy (XPS), temperature-programmed reduction by hydrogen (H_2-TPR), temperature-programmed desorption of ammonia (NH_3-TPD), pulsed CO chemisorption, in situ diffuse reflectance infrared Fourier transform spectroscopy (DRIFTS), and inductively coupled plasma mass spectrometry.

2. MATERIALS AND METHODS

2.1. Sample Preparation. In this study, a Pd/SSZ-13 catalyst was prepared by quantitative ion exchange (QIE) for the adsorption of NO_x from motor vehicle exhaust. First, 0.416 g of palladium nitrate, 0.43 g of ethylhydrazine, and 0.23 g of methyl nitrite were added to a 250 mL beaker, followed by the addition of 120 mL of deionized water. This solution was ultrasonicated for 30 min and stirred at room temperature for 30 min. 10 g of commercial SSZ-13 zeolite (silicon-to-aluminum ratio of 14) (purchased from Passion) was further added, and the solution was continuously stirred. The solution was placed in a constant-temperature water bath, heated to 95 °C, and stirred for another 5 h. The filtered solid was washed with DI water. Furthermore, the solution was dried at 80 °C for 24 h after the reaction and calcined at 550 °C for 5 h to obtain Pd/SSZ-13 catalyst powder,

denoted as Pd(13)-QIE. For comparison with existing PNA technologies, a Pd/SSZ-13 catalyst with Pd loading was prepared using the traditional incipient wetness impregnation method. A $Pd(NO_3)_2$ solution containing 0.075 g of the precious metal Pd was loaded into 10 g of SSZ-13 with a $Pd(NO_3)_2$ solution volume of 9.66 mL, followed by intermittent stirring with a glass rod for 8 h at room temperature, and the prepared catalyst was expressed as Pd(13)-IWI. Finally, the sample was crushed and sieved through a 40−60 mesh for later use before being used to assess the catalytic activity.

2.2. Sample Characterization. The catalysts were characterized by XRD, XPS, ICP-MS, AC-HAADF-STEM, DRIFT, BET, NH_3-TPD, H_2-TPR, and pulsed CO chemisorption, and the detailed characterization parameters are described in the Supporting Information.

2.3. Catalyst Evaluation. The adsorption performance of the NO_x catalyst was evaluated using a simulated motor vehicle exhaust fixed-bed sample evaluation device, which was mainly composed of gas distribution, heating, and detection systems. The heating system uses three thermocouples in the front, middle, and rear to control the catalyst temperature and reduce the temperature error in the sample. The sample was pretreated before the experiment to remove impurities. The details are described in the Supporting Information.

3. RESULTS AND DISCUSSION

3.1. Crystal Structure and Properties. XRD measurements are commonly employed to analyze the structural properties of crystals. Figure 1 (a) shows that all samples exhibit identical CHA diffraction peaks at 2θ values of 9.7, 20.9, and 31.1°. This suggests that various preparation methods did not alter the ordered structure of the catalyst support. Additionally, in the XRD spectra of all samples, there was no discernible PdO peak at 33.9°.[28,29] Through closer inspection, the characteristic peak of PdO at $2\theta = 33.9°$ was found to be weaker in Pd(13)-QIE compared to that in Pd(13)-IWI, indicating that the Pd(13)-QIE catalyst had larger number of Pd entering the zeolite framework, with a small amount of Pd existing on the surface of the zeolite in the form of PdO. Therefore, the Pd/SSZ-13 catalyst prepared by quantitative ion-exchange method exhibited higher dispersion. The Pd(13)-QIE catalyst was hydrothermally aged (HTA) at 800 °C in a 10% water quartz tube for 24 h. The results in Figure 1b show that the catalyst support did not alter the ordered structure before and after the Pd (13) -QIE catalyst aging at 800 °C after hydrothermal aging. Notably, the PdO diffraction peak at $2\theta =$

33.9° decreased, indicating further dispersion of Pd in the Pd(13)-QIE catalyst after hydrothermal treatment.

To investigate the influence of the preparation method on Pd, STEM images were obtained for all the samples, as shown in Figure 2. The dark contrasts in the STEM image of Pd/SSZ-13
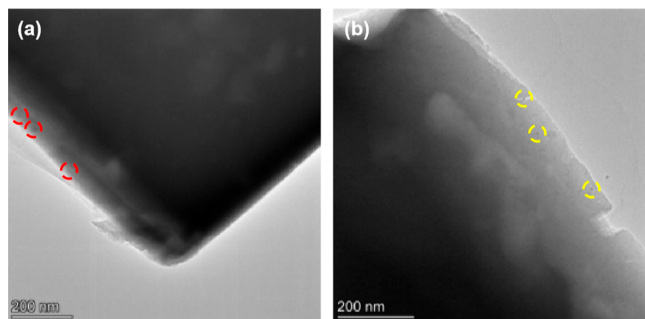
Figure 2. STEM images of (a) Pd(13)-IWI and (b) Pd(13)-QIE.

suggest the presence of well-dispersed Pd species within the pure catalyst. Notably, Pd(13)-IWI displayed a pattern of larger PdO nanoparticles, as indicated by the red dotted line in Figure 2a.[30,31] However, the particles were smaller in the Pd(13)-QIE sample, as indicated by the yellow dotted line in Figure 2b. This implied that a small amount of Pd was present as PdO in the Pd(13)-QIE sample, and the particles were small and did not form large PdO clusters. To further observe the distribution of Pd in the Pd(13)-QIE catalyst from a microscopic perspective, the Pd(13)-QIE catalyst was characterized by AC-HAADF-STEM images and corresponding EDS mapping, and the results are shown in Figure 3; throughout the SSZ-13 crystal, a uniform distribution of silicon and aluminum can be observed, a small number of PdO nanoparticles with sizes in the range of 0.5−1 nm appeared on the catalyst surface, and no large PdO clusters were formed. The majority of Pd existed in the zeolite pores in an ionic form, consistent with the results shown in Figure 2.
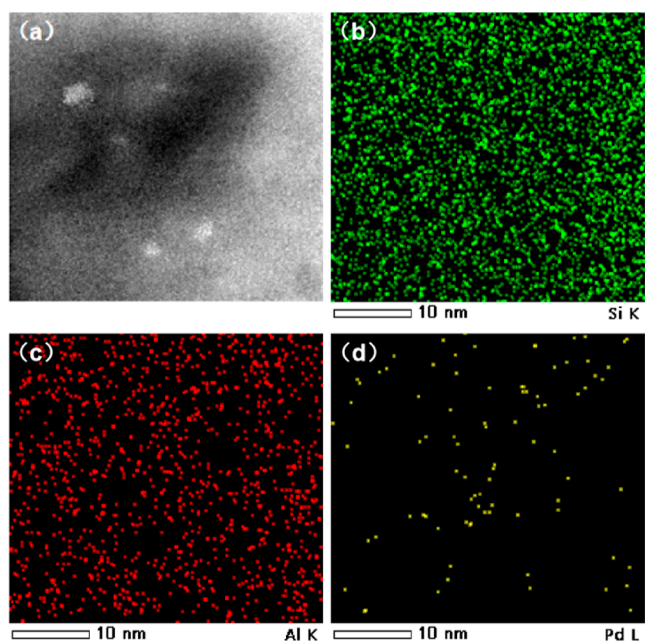
Figure 3. AC-HAADF-STEM images(a) and corresponding EDS mapping (b−d) of Pd(13)-QIE.

3.2. Chemical Properties. The Pd(13)-QIE and Pd(13)-IWI catalysts were characterized by ICP-MS to determine the chemical compositions. As shown in Table 1, the theoretical loading amounts of the two catalysts were 0.75 wt % each. The actual loading amounts of Pd(13)-IWI and Pd(13)-QIE catalysts were 0.748 and 0.742 wt %, respectively. The small difference between the two indicated that a small amount of Pd was distributed in the supernatant during the preparation of the Pd(13)-QIE catalyst, almost achieving quantitative loading of Pd. This also indicated that the quantitative ion-exchange method could achieve a high dispersion of the precious metal Pd in small-pore zeolite SSZ-13.

The Pd(13)-QIE and Pd(13)-IWI catalysts were characterized by N_2 physisorption to understand their structural properties. As shown in Table 1, the surface area of Pd(13)-IWI was 418.04 m^2 g^{-1}, with a microporous volume of 0.20 cm^3 g^{-1}. However, the surface area of Pd(13)-QIE was 511.48 m^2 g^{-1} (an increase of 22.35% compared to Pd(13)-IWI) with a pore volume of 0.25 cm^3 g^{-1} (an increase of 25%). Compared to the blank SSZ-13 support, the Pd(13)-IWI catalyst showed a more significant decrease in the specific surface area and pore volume. Based on the XRD and STEM data analyses, it was hypothesized that this phenomenon might have been caused by the attachment of larger PdO clusters formed on the surface of the Pd(13)-IWI catalyst, blocking the pores on the zeolite surface. Both catalysts exhibited type I isotherms, indicating that the zeolite structure did not change and that more Pd ions existed in Pd(13)-QIE than in Pd(13)-IWI (Figure S1). In the Pd(13)-QIE catalyst, Pd mainly existed in the form of ions inside the zeolite cage and in the pore structure. There were very few Pd clusters on the zeolite surface, and the particles were small and did not block the surface pores of the zeolite; therefore, it had a relatively large specific surface area.

To better understand the effect of the preparation method on the state of Pd in the Pd/zeolite samples, XPS was used to detect the oxidation state of Pd.[18,28] The Pd 3d spectrum is shown in Figure 4. In the Pd/SSZ-13 samples prepared by both methods, Pd(II) and Pd(IV) coexisted. The high-intensity peaks at 336 ($3d_{5/2}$) and 341.4 eV ($3d_{3/2}$) [Pd(II), 57.84%] for Pd(13)-IWI were attributed to Pd^{2+} in Pd-SSZ-13, and the high-intensity peaks at 338.9 ($3d_{5/2}$) and 344.3 eV ($3d_{3/2}$) [Pd(IV), 42.16%] were attributed to Pd^{4+} in Pd-SSZ-13. For the Pd(13)-QIE catalyst, the high-intensity peaks at 336 ($3d_{5/2}$) and 341.4 eV ($3d_{3/2}$) [Pd(II), 80.61%] could be attributed to Pd^{2+} in Pd-SSZ-13, while the peaks at 338.9 ($3d_{5/2}$) and 344.3 eV ($3d_{3/2}$) [Pd(IV), 19.39%] could be attributed to Pd^{4+} in Pd-SSZ-13.[18,32] Compared to the quantitative ion-exchange method, the Pd/SSZ-13 catalyst prepared by the incipient wetness impregnation method contained more Pd(IV) (42.16%) after deconvolution. Based on the fact that the Pd(13)-IWI catalyst contained a higher concentration of Pd(IV), Pd mainly existed in the form of clusters on the external surface. According to the above characterization analysis, Pd(IV) is believed to exist in the form of PdO_2 clusters on the external surface.

The states of Pd in Pd(13)-IWI and Pd(13)-QIE were further investigated using FTIR spectroscopy with NO and CO probe molecules (Figure 5). We summarize the correspondence between the peak center and Pd species in NO-DRIFTS and CO-DRIFTS spectra and list the results in Table 2. Compared to Pd(13)-IWI, the Pd(13)-QIE catalyst exhibited a higher distribution of Pd^{2+} ions. Literature suggests that well-dispersed Pd^{2+} ions in Pd/SSZ-13 are the dominant species low-temperature NO adsorption.[14,22,40−42] To gain deeper insight

Table 1. ICP-MS and XRF Results of Pd(13)-IWI and Pd(13)-QIE

catalyst	Si/Al	Pd theoretical loading (wt %)	ICP Pd loading (wt %)	S_{BET} $(m^2 g^{-1})$	pore volume $(cm^3 g^{-1})$	metal dispersion (%)	average pore diameter (nm)
Pd(13)-IWI	14	0.75	0.748	418.04	0.20	41.31	1.91
Pd(13)-QIE	14	0.75	0.742	511.48	0.25	92.13	1.93
SSZ-13	14	-	-	550.37	0.27		1.92
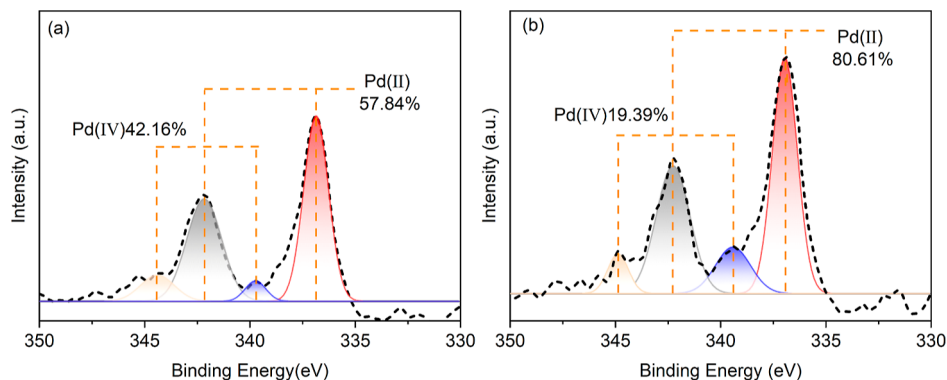
Figure 4. Pd 3d XPS spectra of (a) Pd(13)-IWI and (b) Pd(13)-QIE.
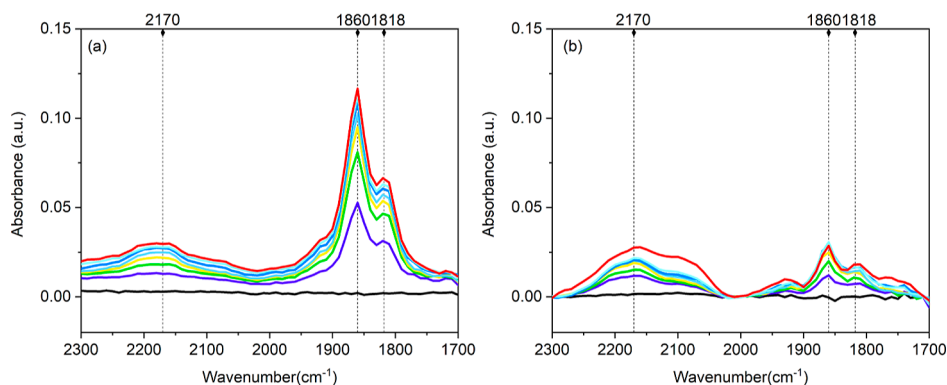
Figure 5. In situ DRIFTS spectra of (a) Pd(13)-QIE and (b) Pd(13)-IWI samples with 1000 ppm of NO in N_2 measured at 100 °C. Total flow rate was 100 mL min^{-1}.

Table 2. Correspondence between the Peak Center and Pd Species in the NO-DRIFTS and CO-DRIFTS Spectra

adsorbate	wavenumber (cm^{-1})	Pd species	refs
NO	2170	NO$^+$ species adsorbed on the support	[16,33]
	1860	Pd^{2+}-NO	[24,34]
	1818	Pd$^+$-NO	[19]
CO	2171/2161	Pd^{2+}-CO	[35−37]
	2148	Pd^{2+}(OH)CO	[28,38,39]
	2105	Pd^{0}O−CO	[7,35]

into the adsorption sites in Pd(13)-QIE, we analyzed the state of Pd in the Pd/SSZ-13 catalysts prepared by various methods using NO probe molecules through FTIR spectroscopy. The NO adsorption properties of the catalysts were evaluated at 100 °C. Initially, each sample underwent preoxidation at 550 °C in a 10% O_2 environment. This was followed by cooling in a nitrogen atmosphere down to 100 °C, with continuous sampling over increasing time intervals. Figure 5 presents a series of DRIFT spectra recorded during NO adsorption on Pd/SSZ-13 catalysts prepared through different methods at 100 °C. These spectra display the function of adsorption time within the 1700−2300 cm^{-1} range.

The spectra from the Pd/SSZ-13 catalysts, prepared via two different methods, revealed three distinct absorption bands in the NO stretching region. The first, a broad band centered at 2170 cm^{-1}, corresponds to the $v_{N−O}$ vibration of NO$^+$ species outside the zeolite framework.[1] This band is attributed to NO$^+$ species at the cationic positions within the zeolite micropores, formed either through direct electron transfer from NO to cationic Pd(II) species or via the intermediate formation of N_2O_3 (resulting from the reaction of NO$^+$ with NO$_2$).[19] Additionally, two narrower bands were observed at 1860 and 1818 cm^{-1}. Notably, NO adsorbed on reduced Pd clusters/nanoparticles did not exhibit a peak. The 1818 cm^{-1} band is associated with Pd I−NO, likely due to Pd(I)−NO species formed by electron transfer from the free radical NO to Pd(II). The band at 1860 cm^{-1} is ascribed to Pd(II)−NO.[16,33] The infrared spectrum of the Pd(13)-QIE catalyst with NO adsorption in Figure 5a shows a maximum peak at approximately 1860 cm^{-1} and a shoulder at 1818 cm^{-1}, both attributed to the nitrite complex on the Pd species. This clearly indicated the presence of Pd^{2+} ions in SSZ-13. The infrared spectrum of the Pd(13)-IWI catalyst without NO adsorption showed relatively

lower intensity peaks at approximately 1860 and 1818 cm^{-1} (Figure 5b), further confirming that the Pd/SSZ-13 catalyst prepared by the quantitative ion-exchange method had more number of Pd^{2+} ions. In addition, Pd(13)-QIE-A was characterized under the same conditions, and the results are presented in Figure S2. Compared to Pd(13)-QIE-F, Pd(13)-QIE-A contained more Pd$^+$-NO, combined with NO$_x$ storage and release curves for Pd(13)-QIE-F and Pd(13)-QIE-A. Pd$^+$-NO might have caused a decrease in the desorption temperature. As shown in Figure S3, CO adsorption mainly formed Pd^{2+}(CO)$_2$, Pd^{2+}(CO), Pd$^+$(CO), Pd^{0+}CO, and Pd(13)-QIE with the highest dispersion.[35] In addition, the metal dispersion was measured by pulsed CO chemisorption, and the domain size was estimated from the dispersion data (Table 1). It is worth noting that the dispersion of precious metal Pd in the Pd(13)-QIE catalyst prepared by quantitative ion-exchange method is much greater than that of Pd(13)-IWI. This is consistent with the observations of CO-DRIFTS.[12]

The effect of the preparation method on Pd species was observed by TEM; however, the high-energy electrons used in STEM might have destroyed the micropores of SSZ-13 and thus severely induce Pd sintering.[1] To more accurately analyze the Pd status in samples, H$_2$-TPR characterization of SSZ-13, Pd(13)-IWI, and Pd(13)-QIE was performed, and the results are shown in Figure 6. The H$_2$-TPR profile of Pd(13)-IWI showed two
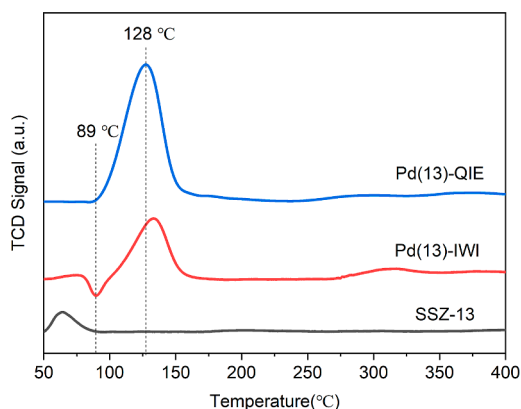
Figure 6. H$_2$-TPR profiles of Pd(13)-QIE and Pd(13)-IWI.

reduction peaks, including a negative peak at 89 °C (due to the decomposition of PdH$_x$) and a positive peak at 128 °C (attributed to the reduction of isolated Pd cations), where PdH$_x$ is formed by the reduction of bulk PdO to metallic Pd and conversion of metallic Pd to PdH$_x$ in the presence of H$_2$.[28] For Pd(13)-QIE, negative peaks originating from PdH$_x$ decomposition were not observed. Notably, the positive peak at approximately 128 °C was stronger, with a peak area of 226.6, whereas the peak area of the positive peak in Pd(13)-IWI was only 85.7. The combined characterization results of XRD, STEM, and ICP-MS show that there is very little or no PdO in Pd(13)-QIE and that Pd mainly exists in the ionic form.

NH$_3$-TPD was performed to explore the effects of the different preparation methods on the acidic sites of the catalysts. As shown in Figure 7, Pd(13)-QIE and Pd(13)-IWI both showed two NH$_3$ desorption peaks, with peak I around ~150 °C attributed to Lewis acid sites and peak II around ~480 °C attributed to Brønsted acid sites.[30] The two catalysts' peak I basically coincided, and the NH$_3$ desorption differences were 0.5244 and 0.5535 μmol·g^{-1}, respectively, whereas peak II was
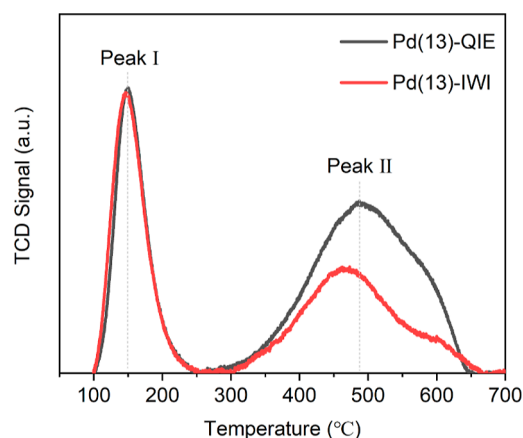
Figure 7. NH$_3$-TPD profiles of Pd(13)-QIE and Pd(13)-IWI.

quite different, and peak II NH$_3$ desorption of Pd(13)-QIE was 1.07 μmol·g^{-1}, which was 1.8 times that of Pd(13)-IWI (Table S1). Pd(13)-QIE had more Brønsted acid sites and contributed to the stability of Pd^{2+} cations and dispersion of Pd species, producing more [Pd(OH)]$^+$ active centers. This result matched with the in situ DRIFTS spectra and proved that [Pd(OH)]$^+$ was the main active center for NO adsorption in Pd(13)-QIE.[43] In addition, the molecular sieve Brønsted acid site could also store NO$_x$ according to this process: 2NO + 1/2O$_2$ + 2 ZH$^+$ ⇌ H$_2$O + 2 Z-NO$^+$.[7]

3.3. Catalytic Performance. Figure 8a shows the NO$_x$ storage and release curves of the Pd(13)-IWI and Pd(13)-QIE catalysts. The experimental procedure for NO$_x$ adsorption and resolution is presented in the Supporting Information. The peak corresponding to NO$_x$ below 500 ppm in the first 10 min at the onset of adsorption indicates the storage of NO$_x$ in the catalyst, and the peak above 500 ppm after the onset of desorption indicates the release of NO$_x$ in the catalyst. The values for the adsorption and desorption of NO$_x$ were calculated using the formula given in the Supporting Information. A large number of published studies on Pd/SSZ-13 are summarized, and various information about the catalyst is compiled in Table 3. Compared to the best PNA materials reported in the literature, even under more severe test conditions, Pd/SSZ-13 prepared in this study still has the best PNA performance.

During storage, when the gas was mixed in the bypass and switched to the reactor, the concentration of NO$_x$ decreased rapidly and finally dropped to the lowest value. With time, the NO$_x$ concentration gradually increased to an initial value of 500 ppm, which lasted for approximately 10 min, where the NO$_x$ storage phase was complete. Subsequently, the reaction tube was heated at a fixed heating rate, and as the temperature increased, NO$_x$ was released. When the temperature rises to approximately 200 °C, the stored NO$_x$ was released. As shown in the graph, the NO$_x$ release curve of Pd(13)-IWI reached a maximum value at approximately 347 °C. Compared to Pd(13)-IWI, Pd(13)-QIE corresponds to a higher peak, even though the maximum peak of the release curve exhibited a 27 °C increase in temperature (374 °C), but the desorption interval did not change considerably. Notably, Pd(13)-QIE exhibited a higher NO$_x$ capture capacity than Pd(13)-IWI throughout the storage phase. The total NO$_x$ adsorptions of Pd(13)-IWI and Pd(13)-QIE were 51.96 and 73.79 μmol·g^{-1} (their NO/Pd values were 0.75 and 1.06), respectively, which was 70.42% of the adsorption capacity of Pd(13)-QIE catalyst. Figure 8b shows the changes in NH$_3$ and
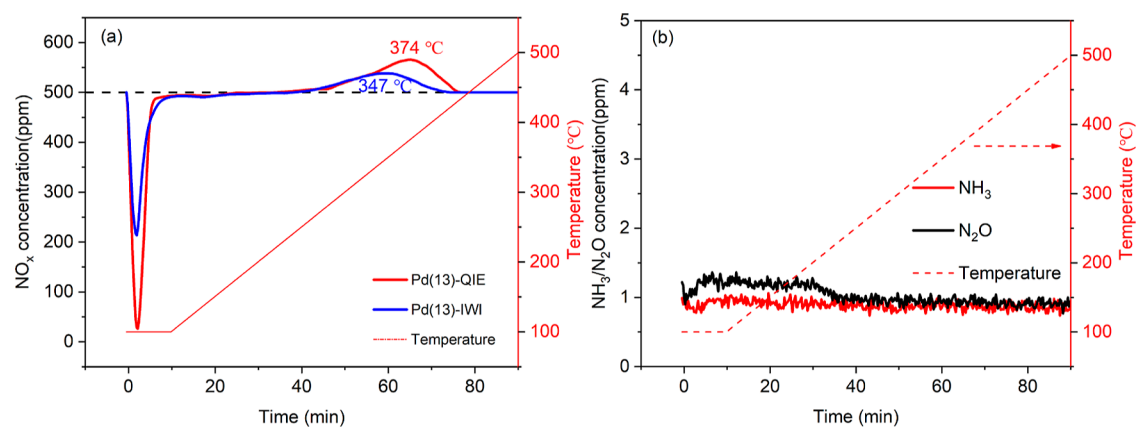
Figure 8. NO$_x$ adsorption at 100 °C for 10 min (after 10 min bypass) followed by TPD (5 °C/min). (a) Pd(13)-IWI and Pd(13)-QIE and (b) NH$_3$ and N$_2$O of Pd(13)-QIE. The feed gas mixture contains 500 ppm of NO$_x$, 10% O$_2$, 5% H$_2$O, and 500 ppm of CO.

Table 3. Comparison of Different Reported PNA Materials in the Literature Studies

material (Si/Al)	NO$_x$ storage ($\mu mol \cdot g^{-1}$)	reaction conditions	GHSV (h^{-1})	adsorption temperature (°C)	refs
0.82 wt %Pd/SSZ-13 (10)	48.3	200 ppm of NO, 10% O$_2$, 5% H$_2$O, balanced with N$_2$	120,000	120	[44]
1 wt %Pd/SSZ-13 (25)	45.6	200 ppm of NOx, 200 ppm of CO, 10% O$_2$, 5% H$_2$O	40,000	100	[38]
1 wt %Pd/SSZ-13 (11)	48	200 ppm of NO, 12% O$_2$, 200 ppm of CO, 5% H$_2$O, 50 ppm of C$_{10}$H$_{22}$, 5% CO$_2$, balanced with N$_2$	150,000	100	[20]
1 wt %Pd/SSZ-13 (7.6)	94.1	210 ppm of NO$_x$, 10% O$_2$, 5% H$_2$O, balanced with N$_2$	30,000	90	[45]
2 wt %Pd/SSZ-13 (35)	25.4	300 ppm NO, 3% O$_2$, 2% CO$_2$, 2.5% H$_2$O, balanced with He	120,000	120	[23]
1 wt %Pd/SSZ-13 (10)	85.6	200 ppm of NO, 10% O$_2$, 5% H$_2$O, balanced with N$_2$	50,000	100	[30]
1 wt %Pd/SSZ-13 (6)	94	200 ppm of NO$_x$, 14% O$_2$, 200 ppm of CO, 3% H$_2$O, balanced with N$_2$	105,000	100	[1]
1 wt %Pd/SSZ-13 (−)	57.1	200 ppm of NO, 15 ppm of NO$_2$, 10% O$_2$, 2.5% H$_2$O, balanced with N$_2$	50,000	110	[34]
1 wt %Pd/SSZ-13 (25)	33.9	200 ppm of NO, 10% O$_2$, 5% H$_2$O, balanced with N$_2$	330,000	100	[39]
2 wt %Pd/SSZ-13 (22.4)	31.1	100 ppm of NO, 9.5% O$_2$, 5% H$_2$O, 5% CO$_2$, balanced with N$_2$	120,000	120	[24]
2 wt %Pd/SSZ-13 (22.4)	30.4	100 ppm of NO, 9.5% O$_2$, 5% H$_2$O, 5% CO$_2$, balanced with N$_2$	120,000	120	[29]
0.75 wt %Pd/SSZ-13 (14)	73.79	500 ppm of NO; 10% O$_2$, 500 ppm of CO, 5% H$_2$O, balanced with N$_2$	40,000	100	this work
3 wt %Pd/SSZ-13 (6)	398.5	500 ppm of NO; 10% O$_2$, 500 ppm of CO, 5% H$_2$O, balanced with N$_2$	40,000	100	this work
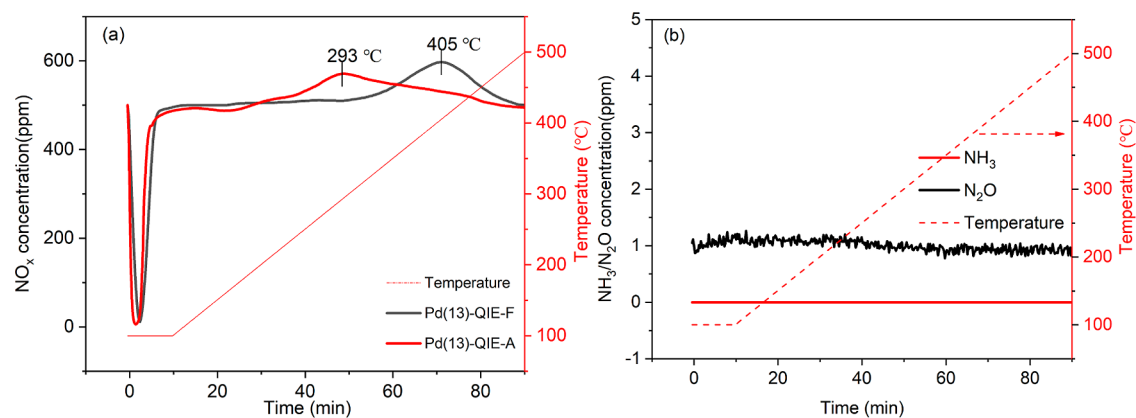
Figure 9. NO$_x$ profiles of (a) Pd(13)-QIE-F and Pd(13)-QIE-A and (b) NH$_3$ and N$_2$O of Pd(13)-QIE-Aging. The feed gas mixture contains 500 ppm of NO$_x$, 10% O$_2$, 5% H$_2$O, and 500 ppm of CO.

N$_2$O throughout the reaction. Only minimal amounts of NH$_3$ and N$_2$O were produced throughout the reaction.

To further investigate the stability and durability of Pd/SSZ-13-QIE for practical applications (Figure 9), it was hydrothermally aged (HTA) at 800 °C in a 10% water quartz tube for 24 h.[44] Aging of the catalyst mainly resulted in the formation of large PdO nanoparticles distributed on the catalyst surface, rather than metallic Pd or small PdO clusters. Since the backbone Al ion was the anchoring point for the Pd ion, meaning

the Pd atom replaced the Brønsted acid proton opposite the Al atom, a portion of Al was removed from the zeolite during hydrothermal aging treatment. This process reduced the number of these anchoring sites.[19] Thus, the PdO and/or Pd(OH)$_2$ moieties moved freely and eventually reunite to form larger PdO clusters. However, it has been reported in the literature that the precious metal Pd is redispersed after hydrothermal aging, and the performance of the catalyst is further improved.[24] As shown in Figure 9a, the hydrothermal

aging performance of the Pd(13)-QIE catalyst was evaluated, and a slight improvement in the catalyst performance was observed, which agrees well with the reported studies. The reason for this performance improvement might be the redispersion of Pd within the zeolite, which further verified the dispersion of Pd after aging, as shown in Figure 1.[29,45,46] Notably, the desorption temperature of the catalyst decreased after aging for fresh samples. The desorption temperature range was 200−400 °C, and the nitrogen oxides adsorbed by PNA could well meet the desorption temperature requirements.

4. CONCLUSIONS

This study investigated the impact of different preparation methods on the loading, dispersibility, and activity of Pd in Pd/SSZ-13 catalysts. We prepared Pd/SSZ-13 samples with identical theoretical loadings using both traditional impregnation and quantitative ion-exchange methods to assess their NO_x adsorption capacities. Characterization techniques like XRD, AC-HAADF-STEM, XPS, H_2-TPR, NH_3-TPD, pulsed CO chemisorption, and FTIR revealed that the Pd in Pd/SSZ-13 catalysts prepared via the quantitative ion-exchange method exhibited superior dispersion, and the dispersion of precious metal Pd was as high as 92.13%, predominantly existing within SSZ-13 zeolite's pores and cages as Pd^{2+}, compared to those prepared by traditional impregnation. ICP-MS results indicated that the Pd(13)-QIE sample achieved nearly complete Pd loading, reaching up to 98.93%. Furthermore, the Pd(13)-QIE's performance remained stable postaging. Our findings suggest that the quantitative ion-exchange method markedly enhances Pd dispersion and loading in SSZ-13 zeolite, thus improving the NO_x adsorption efficiency of Pd/SSZ-13 catalysts. This study offers valuable insights for advancing the quantitative loading and efficacy of precious metals in Pd/SSZ-13.

■ ASSOCIATED CONTENT

Data Availability Statement

No data was used for the research described in the article.

Ⓢ Supporting Information

The Supporting Information is available free of charge at https://pubs.acs.org/doi/10.1021/acsomega.4c01873.

> Additional experimental details, materials, and methods, including detailed characterization methods, evaluation of NOx adsorption performance method, N_2 adsorption isotherms, in situ DRIFTS spectra, and amount of NH_3 desorption from NH_3-TPD (PDF)

■ AUTHOR INFORMATION

Corresponding Authors

Yatao Liu − *National Engineering Laboratory for Mobile Source Emission Control Technology, China Automotive Technology & Research Center Co., Ltd., Tianjin 300300, China;* ⓞ orcid.org/0009-0008-8259-2332; Email: liuyatao@catarc.ac.cn

Zhenguo Li − *National Engineering Laboratory for Mobile Source Emission Control Technology, China Automotive Technology & Research Center Co., Ltd., Tianjin 300300, China;* Email: lizhenguo@catarc.ac.cn

Authors

Kaixiang Li − *National Engineering Laboratory for Mobile Source Emission Control Technology, China Automotive*

Technology & Research Center Co., Ltd., Tianjin 300300, China

Yuankai Shao − *National Engineering Laboratory for Mobile Source Emission Control Technology, China Automotive Technology & Research Center Co., Ltd., Tianjin 300300, China*

Xiaoning Ren − *National Engineering Laboratory for Mobile Source Emission Control Technology, China Automotive Technology & Research Center Co., Ltd., Tianjin 300300, China*

Bingjie Zhou − *National Engineering Laboratory for Mobile Source Emission Control Technology, China Automotive Technology & Research Center Co., Ltd., Tianjin 300300, China*

Anqi Dong − *National Engineering Laboratory for Mobile Source Emission Control Technology, China Automotive Technology & Research Center Co., Ltd., Tianjin 300300, China*

Xi Liu − *National Engineering Laboratory for Mobile Source Emission Control Technology, China Automotive Technology & Research Center Co., Ltd., Tianjin 300300, China*

Cheng Lv − *National Engineering Laboratory for Mobile Source Emission Control Technology, China Automotive Technology & Research Center Co., Ltd., Tianjin 300300, China*

Complete contact information is available at:
https://pubs.acs.org/10.1021/acsomega.4c01873

Author Contributions

Yatao Liu contributed to conceptualization, formal analysis, and writing—original draft. Kaixiang Li contributed to project administration, visualization, and writing—review and editing. Yuankai Shao contributed to supervision and writing—review and editing. Xiaoning Ren contributed to data curation and writing—review and editing. Bingjie Zhou contributed to writing—review and editing. Anqi Dong contributed to methodology and validation. Xi Liu contributed to resources and investigation. Cheng Lv contributed to methodology and validation. Zhenguo Li contributed to supervision, writing—review and editing, and funding acquisition.

Notes

The authors declare no competing financial interest.

■ REFERENCES

(1) Khivantsev, K.; Jaegers, N. R.; Kovarik, L.; Hanson, J. C.; Tao, F.; Tang, Y.; Zhang, X.; Koleva, I. Z.; Aleksandrov, H. A.; Vayssilov, G. N.; Wang, Y.; Gao, F.; Szanyi, J. Achieving Atomic Dispersion of Highly Loaded Transition Metals in Small-Pore Zeolite SSZ-13: High-Capacity and High-Efficiency Low-Temperature CO and Passive NO_x Adsorbers. *Angew. Chem., Int. Ed.* **2018**, *57* (51), 16672−16677.

(2) Ryou, Y.; Lee, J.; Kim, Y.; Hwang, S.; Lee, H.; Kim, C. H.; Kim, D. H. Effect of reduction treatments (H_2 vs. CO) on the NO adsorption ability and the physicochemical properties of Pd/SSZ-13 passive NOx adsorber for cold start application. *Appl. Catal., A* **2019**, *569*, 28−34.

(3) Han, L.; Cai, S.; Gao, M.; Hasegawa, J.-y.; Wang, P.; Zhang, J.; Shi, L.; Zhang, D. Selective Catalytic Reduction of NOx with NH_3 by Using Novel Catalysts: State of the Art and Future Prospects. *Chem. Rev.* **2019**, *119* (19), 10916−10976.

(4) Jia, L.; Liu, J.; Huang, D.; Zhao, J.; Zhang, J.; Li, K.; Li, Z.; Zhu, W.; Zhao, Z.; Liu, J. Interface Engineering of a Bifunctional Cu-SSZ-13@CZO Core-Shell Catalyst for Boosting Potassium Ion and SO$_2$ Tolerance. *ACS Catal.* **2022**, *12* (18), 11281−11293.

(5) Jia, L.; Liu, J.; Cheng, H.; Zhao, Z.; Liu, J. Review of Core-shell structure zeolite-based catalysts for NOx emission control. *J. Environ. Sci.* **2025**, *150*, 451−465.

(6) Li, Y.; Chen, D.; Xu, X.; Wang, X.; Kang, R.; Fu, M.; Guo, Y.; Chen, P.; Li, Y.; Ye, D. Cold-Start NO$_x$ Mitigation by Passive Adsorption Using Pd-Exchanged Zeolites: From Material Design to Mechanism Understanding and System Integration. *Environ. Sci. Technol.* **2023**, *57* (9), 3467−3485.

(7) Yu, Q.; Chen, X.; Bhat, A.; Tang, X.; Yi, H.; Lin, X.; Schwank, J. W. Activation of passive NOx adsorbers by pretreatment with reaction gas mixture. *Chem. Eng. J.* **2020**, *399*, 125727.

(8) Gu, Y.; Sinha Majumdar, S.; Pihl, J. A.; Epling, W. S. Investigation of NO adsorption and desorption phenomena on a Pd/ZSM-5 passive NOx adsorber. *Appl. Catal., B* **2021**, *298*, 120561.

(9) Xu, L.; Zhao, F.; Wei, H.; Zhao, P.; Qian, W.; Qian, M. The Development of a Zeolite-Based Cold-Start Catalyst (CSC) for a Conventional China 6b Vehicle in Meeting the Next More Stringent Chinese Vehicle Emission Standards. In *SAE Technical Paper Series*, 2023.

(10) Lee, J.; Kim, Y.; Hwang, S.; Lee, E.; Lee, H.; Kim, C. H.; Kim, D. H. Deactivation of Pd/Zeolites passive NOx adsorber induced by NO and H$_2$O: Comparative study of Pd/ZSM-5 and Pd/SSZ-13. *Catal. Today* **2021**, *360*, 350−355.

(11) Wu, Y.; Wang, J.; Chen, Z.; Zhu, Y.; Yu, M.; Wang, C.; Zhai, Y.; Wang, J.; Shen, G.; Shen, M. A novel material for passive NO adsorber: Ce-based BEA zeolite. *J. Rare Earths* **2023**, *41* (8), 1163−1170.

(12) Jia, L.; Shao, Y.; Li, Z.; Li, K.; Ren, X.; Wu, H.; Li, H.; Cheng, K.; Cheng, H.; Liu, J.; Liu, J. Atomically Dispersed Pt-Triggered CZO/Cu-SSZ-13 Coupling Catalyst for the Efficient Low-Temperature Selective Catalytic Reduction of NO$_x$. *ACS ES&T Eng.* **2024**, *4*, 1007−1015.

(13) Lee, J.; Theis, J. R.; Kyriakidou, E. A. Vehicle emissions trapping materials: Successes, challenges, and the path forward. *Appl. Catal., B* **2019**, *243*, 397−414.

(14) Moliner, M.; Corma, A. From metal-supported oxides to well-defined metal site zeolites: the next generation of passive NOx adsorbers for low-temperature control of emissions from diesel engines. *React. Chem. Eng.* **2019**, *4* (2), 223−234.

(15) Gu, Y.; Marino, S.; Cortés-Reyes, M.; Pieta, I. S.; Pihl, J. A.; Epling, W. S. Integration of an Oxidation Catalyst with Pd/Zeolite-Based Passive NOx Adsorbers: Impacts on Degradation Resistance and Desorption Characteristics. *Ind. Eng. Chem. Res.* **2021**, *60* (18), 6455−6464.

(16) Khivantsev, K.; Gao, F.; Kovarik, L.; Wang, Y.; Szanyi, J. Molecular Level Understanding of How Oxygen and Carbon Monoxide Improve NOx Storage in Palladium/SSZ-13 Passive NOx Adsorbers: The Role of NO$^+$ and Pd(II)(CO)(NO) Species. *J. Phys. Chem. C* **2018**, *122* (20), 10820−10827.

(17) Cheng, H.; Tang, X.; Yi, H.; Pan, R.; Zhang, J.; Gao, F.; Yu, Q. Application progress of small-pore zeolites in purifying NOx from motor vehicle exhaust. *Chem. Eng. J.* **2022**, *449*, 137795.

(18) Zheng, Y.; Kovarik, L.; Engelhard, M. H.; Wang, Y.; Wang, Y.; Gao, F.; Szanyi, J. Low-Temperature Pd/Zeolite Passive NO$_x$ Adsorbers: Structure, Performance, and Adsorption Chemistry. *J. Phys. Chem. C* **2017**, *121* (29), 15793−15803.

(19) Khivantsev, K.; Jaegers, N. R.; Kovarik, L.; Hu, J. Z.; Gao, F.; Wang, Y.; Szanyi, J. Palladium/Zeolite Low Temperature Passive NOx Adsorbers (PNA): Structure-Adsorption Property Relationships for Hydrothermally Aged PNA Materials. *Emiss. Control Sci. Technol.* **2020**, *6* (2), 126−138.

(20) Chen, H.-Y.; Collier, J. E.; Liu, D.; Mantarosie, L.; Durán-Martín, D.; Novák, V.; Rajaram, R. R.; Thompsett, D. Low Temperature NO Storage of Zeolite Supported Pd for Low Temperature Diesel Engine Emission Control. *Catal. Lett.* **2016**, *146* (9), 1706−1711.

(21) Gupta, A.; Kang, S. B.; Harold, M. P. NOx uptake and release on Pd/SSZ-13: Impact Of Feed composition and temperature. *Catal. Today* **2021**, *360*, 411−425.

(22) Ilmasani, R. F.; Yao, D.; Ho, P. H.; Bernin, D.; Creaser, D.; Olsson, L. Deactivation of phosphorus-poisoned Pd/SSZ-13 for the passive adsorption of NOx. *J. Environ. Chem. Eng.* **2022**, *10* (3), 107608.

(23) Lee, J.; Ryou, Y.; Hwang, S.; Kim, Y.; Cho, S. J.; Lee, H.; Kim, C. H.; Kim, D. H. Comparative study of the mobility of Pd species in SSZ-13 and ZSM-5, and its implication for their activity as passive NOx adsorbers (PNAs) after hydro-thermal aging. *Catal. Sci. Technol.* **2019**, *9* (1), 163−173.

(24) Ryou, Y.; Lee, J.; Cho, S. J.; Lee, H.; Kim, C. H.; Kim, D. H. Activation of Pd/SSZ-13 catalyst by hydrothermal aging treatment in passive NO adsorption performance at low temperature for cold start application. *Appl. Catal., B* **2017**, *212*, 140−149.

(25) Wang, Y.; Shi, X.; Liu, Z.; Shan, Y.; Shi, W.; Yu, Y.; He, H. The study of Pd-SSZ-13 as low-temperature passive NO adsorber materials: High dispersal of Pd in small-pore CHA zeolites by thermal treatment. *Appl. Catal., B* **2023**, *324*, 122254.

(26) Zhao, H.; Hill, A. J.; Ma, L.; Bhat, A.; Jing, G.; Schwank, J. W. Progress and future challenges in passive NO adsorption over Pd/zeolite catalysts. *Catal. Sci. Technol.* **2021**, *11* (18), 5986−6000.

(27) Yu, Q.; Cheng, H.; Pan, R.; Li, Z.; Yi, H.; Gao, F.; Zhou, Y.; Zhang, J.; Yao, Y.; Tang, X. Correlation between zeolitic particle size and the low-temperature NOx storage capacity of Pd/ZSM-11 passive NOx adsorber. *J. Solid State Chem.* **2023**, *326*, 124189.

(28) Chen, D.; Lei, H.; Xiong, W.; Li, Y.; Ji, X.; Yang, J.-Y.; Peng, B.; Fu, M.; Chen, P.; Ye, D. Unravelling Phosphorus-Induced Deactivation of Pd-SSZ-13 for Passive NO$_x$ Adsorption and CO Oxidation. *ACS Catal.* **2021**, *11* (22), 13891−13901.

(29) Ryou, Y.; Lee, J.; Lee, H.; Kim, C. H.; Kim, D. H. Effect of various activation conditions on the low temperature NO adsorption performance of Pd/SSZ-13 passive NOx adsorber. *Catal. Today* **2019**, *320*, 175−180.

(30) Li, D.; Yang, G.; Chen, M.; Pang, L.; Guo, Y.; Yu, J.; Li, T. Na co-cations promoted stability and activity of Pd/SSZ-13 for low-temperature NO adsorption. *Appl. Catal., B* **2022**, *309*, 121266.

(31) Gu, Y.; Zelinsky, R. P.; Chen, Y.-R.; Epling, W. S. Investigation of an irreversible NOx storage degradation Mode on a Pd/BEA passive NOx adsorber. *Appl. Catal., B* **2019**, *258*, 118032.

(32) Wang, A.; Xie, K.; Kumar, A.; Kamasamudram, K.; Olsson, L. Layered Pd/SSZ-13 with Cu/SSZ-13 as PNA - SCR dual-layer monolith catalyst for NOx abatement. *Catal. Today* **2021**, *360*, 356−366.

(33) Matarrese, R.; Castoldi, L.; Morandi, S.; Ticali, P.; Valsania, M. C.; Lietti, L. NO adsorption/desorption pathways over Pd/SSZ-13 low temperature NOx adsorbers investigated by operando FT-IR spectroscopy and microreactor study. *Appl. Catal., B* **2023**, *331*, 122723.

(34) Shan, Y.; Sun, Y.; Li, Y.; Shi, X.; Shan, W.; Yu, Y.; He, H. Passive NO Adsorption on Hydrothermally Aged Pd-Based Small-Pore Zeolites. *Top. Catal.* **2020**, *63* (9−10), 944−953.

(35) Song, I.; Khivantsev, K.; Wang, Y.; Szanyi, J. Elucidating the Role of CO in the NO Storage Mechanism on Pd/SSZ-13 with in Situ DRIFTS. *J. Phys. Chem. C* **2022**, *126* (3), 1439−1449.

(36) Yao, D.; Ho, P. H.; Ilmasani, R. F.; Wurzenberger, J. C.; Glatz, T.; Creaser, D.; Olsson, L. Enhanced CO resistance of Pd/SSZ-13 for passive NOx adsorption. *Chem. Eng. J.* **2023**, *460*, 141681.

(37) Wang, A.; Lindgren, K.; Di, M.; Bernin, D.; Carlsson, P.-A.; Thuvander, M.; Olsson, L. Insight into hydrothermal aging effect on Pd sites over Pd/LTA and Pd/SSZ-13 as PNA and CO oxidation monolith catalysts. *Appl. Catal., B* **2020**, *278*, 119315.

(38) Chen, Z.; Wang, M.; Wang, J.; Wang, C.; Wang, J.; Li, W.; Shen, M. Investigation of crystal size effect on the NOx storage performance of Pd/SSZ-13 passive NOx adsorbers. *Appl. Catal., B* **2021**, *291*, 120026.

(39) Khivantsev, K.; Jaegers, N. R.; Koleva, I. Z.; Aleksandrov, H. A.; Kovarik, L.; Engelhard, M.; Gao, F.; Wang, Y.; Vayssilov, G. N.; Szanyi, J. Stabilization of Super Electrophilic Pd^{+2} Cations in Small-Pore SSZ-13 Zeolite. *J. Phys. Chem. C* **2020**, *124* (1), 309−321.

(40) Castoldi, L.; Morandi, S.; Ticali, P.; Matarrese, R.; Lietti, L. An Assessment of Zeolite Framework Effect for Low-Temperature NOx Adsorbers. *Catalysts* **2023**, *13* (6), 962.

(41) Wang, Z.; Chen, B.; Zhao, Q.; Crocker, M.; Li, Y.; Shi, C. Metal-support interaction induced atomic dispersion and redispersion of Pd on CeO$_2$ for passive NOx adsorption. *Chem. Eng. J.* **2023**, *470*, 144080.

(42) Khivantsev, K.; Jaegers, N. R.; Kovarik, L.; Prodinger, S.; Derewinski, M. A.; Wang, Y.; Gao, F.; Szanyi, J. Palladium/Beta zeolite passive NOx adsorbers (PNA): Clarification of PNA chemistry and the effects of CO and zeolite crystallite size on PNA performance. *Appl. Catal., A* **2019**, *569*, 141−148.

(43) Wang, Y.; Yong, X.; Rong, M.; Zheng, J.; Zhao, H. Recent advances in catalytic automotive emission control: Passive NO storage at low temperatures. *J. Chin. Chem. Soc.* **2020**, *67* (9), 1530−1543.

(44) Kim, Y.; Hwang, S.; Lee, J.; Ryou, Y.; Lee, H.; Kim, C. H.; Kim, D. H. Comparison of NOx Adsorption/Desorption Behaviors over Pd/CeO$_2$ and Pd/SSZ-13 as Passive NOx Adsorbers for Cold Start Application. *Emiss. Control Sci. Technol.* **2019**, *5* (2), 172−182.

(45) Theis, J. R.; Ura, J.; Getsoian, A. B.; Prikhodko, V. Y.; Thomas, C. R.; Pihl, J. A.; Lardinois, T. M.; Gounder, R.; Wei, X.; Ji, Y.; Pace, R. B.; Crocker, M. Effect of framework Al pairing on NO storage properties of Pd-CHA passive NOx adsorbers. *Appl. Catal., B* **2023**, *322*, 122074.

(46) Toops, T.; Binder, A.; Kunal, P.; Kyriakidou, E.; Choi, J.-S. Analysis of Ion-Exchanged ZSM-5, BEA, and SSZ-13 Zeolite Trapping Materials under Realistic Exhaust Conditions. *Catalysts* **2021**, *11* (4), 449.